

On the Relationship Between Wind, SST, and the Thermocline in the Seychelles–Chagos Thermocline Ridge

Ebenezer S. Nyadjro¹, Tommy G. Jensen, James G. Richman, and Jay F. Shriver

Abstract—This letter investigates the relationship between wind, sea surface temperature (SST), and thermocline in the Seychelles–Chagos Thermocline Ridge (SCTR, 5°S–10°S, 50°E–80°E) using a combination of satellite data and a reanalysis version of the HYbrid Coordinate Ocean Model from 1993 to 2012. The asymmetry of this relationship during positive and negative Indian Ocean Dipole (IOD) events and the impacts on the SST–thermocline depth (represented by the 20 °C isotherm depth, D20) relationship—are examined. On interannual timescales, an asymmetric relation between SST and zonal wind stress causes a strengthening of easterlies that enhances anticyclonic wind stress curl and local Ekman downwelling, which in turn deepens the D20 and increases the heat content during positive IOD (PIOD) events. In contrast, during negative IOD (NIOD) events, the winds reverse to be westerlies and cause a three times greater impact on remotely generated upwelling Rossby waves. Subsequently, these asymmetric relations cause an asymmetric D20–SST feedback in the SCTR such that a shoaling D20 is ~2.5 times more effective at lowering SST during NIOD events than a deepening D20 is at raising the SST during PIOD events. The changes to D20 are observed to extend into the year following IOD events, persisting into the end of the year following a PIOD event (due to stronger asymmetric reinforcing effects of warm SST anomalies on zonal wind anomalies) but only to May–June of the year following NIOD events.

Index Terms—Altimetry, HYbrid Coordinate Ocean Model (HYCOM), Indian Ocean Dipole (IOD), ocean–atmosphere coupling, Rossby waves, sea surface temperature (SST), thermocline depth, winds.

I. INTRODUCTION

THE exchange of heat between the ocean surface and subsurface is important for variations in air–sea interactions. Vertical migration of the thermocline (represented by the depth of the 20 °C isotherm, D20) causes variations in the upper ocean heat storage. Anomalies in subsurface temperatures in turn affect sea surface temperature (SST) as cooler waters are upwelled into the surface layer, a process referred to as the thermocline feedback mechanism [1], [2].

Manuscript received July 21, 2017; revised September 13, 2017; accepted October 10, 2017. Date of publication November 7, 2017; date of current version December 4, 2017. This work was supported in part by the Office of Naval Research (ONR) through the Earth Systems Prediction Capability and in part by the ONR-Direct Research Initiative Northern Arabian Sea Circulation-autonomous research projects under Grant 73-4347-34-5. (Corresponding author: Ebenezer S. Nyadjro.)

E. S. Nyadjro is with the Department of Physics, University of New Orleans, New Orleans, LA 70148 USA (e-mail: enyadjro@uno.edu).

T. G. Jensen and J. F. Shriver are with the Naval Research Laboratory, Stennis Space Center, MS 39529 USA.

J. G. Richman is with the Center for Ocean-Atmospheric Prediction Studies, Florida State University, Tallahassee, FL 32306 USA.

Color versions of one or more of the figures in this letter are available online at <http://ieeexplore.ieee.org>.

Digital Object Identifier 10.1109/LGRS.2017.2762961

This feedback impacts air–sea interactions in the region and beyond. A dynamic air–sea interaction region exists in the tropical southwestern Indian Ocean (SWIO). Within this region is a thermocline ridge or dome known as the Seychelles–Chagos Thermocline Ridge (SCTR, 5°S–10°S, 50°E–80°E; Fig. 1), where the vertical temperature gradient in the thermocline is greater than that in surrounding areas. The SCTR is characterized by a quasi-permanent upwelling regime that is often associated with thermocline shoaling (Fig. 1(b) and (c); [1], [3], [4]). The shallow thermocline and a rather unique high SST in the SWIO result in a strong ocean–atmosphere coupling that creates climatic impacts on several timescales. These include influence on tropical cyclones [1], the Madden–Julian oscillation, an intraseasonal, eastward-propagating coupled atmospheric–oceanic mode [5], and how the Indian Ocean Dipole (IOD) and/or El Niño Southern Oscillation (ENSO)-induced SST anomalies (SSTAs) affect the monsoon onset date [1]. As a result, the ocean–atmosphere interactions in the SWIO have regional consequences that affect the socioeconomic livelihood of people in the countries located along the Indian Ocean rim.

On interannual timescales, the Indian Ocean is impacted by the IOD [6], [7] and ENSO [1]. The IOD peaks during September–November (SON), whereas the ENSO peaks during November–January (NDJ) in the Indian Ocean [6], [8]. During a positive IOD (PIOD) event, the winds along and south of the equator are easterly, and SST and rainfall near the coasts of Java and Sumatra are anomalously low while those in the western Indian Ocean are anomalously high. Anomalies of opposite sign are observed during the occurrence of negative IOD (NIOD) events [6], [7]. When an El Niño event occurs, the whole tropical region experiences high SSTAs in the Indian Ocean, whereas the reverse happens during a La Niña event [8]. While the IOD is an intrinsic mode of Indian Ocean variability, it has been reported to co-occur with some ENSO events [6]–[9].

There is an asymmetry between PIOD and NIOD events in the eastern Indian Ocean which causes differences in the amplitudes of oceanic and atmospheric manifestations of these climatic events. For example, SSTAs of larger magnitude are observed during PIOD events than during NIOD events in the eastern Indian Ocean [10], [11]. The existence of this asymmetry in SSTA and its impact on the ocean–atmosphere coupling in the western Indian Ocean have not been explored. Such an asymmetry in SST could cause differing magnitudes and dynamics of the interactions between the ocean surface and thermocline.

In this letter, we use a combination of satellite data and the HYbrid Coordinate Ocean Model (HYCOM) reanalysis

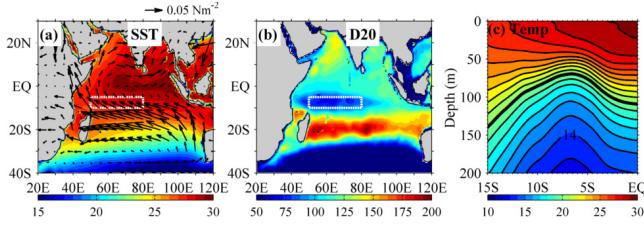


Fig. 1. Annual mean. (a) SST (color shading, °C) and wind stress (vectors, $\text{N}\cdot\text{m}^{-2}$). (b) Thermocline depth (m). White boxes show the SCTR (5°S – 10°S , 50°E – 80°E). (c) Latitudinal variation of annual mean temperature (°C) in the upper 200 m averaged over 50°E – 80°E . Contour interval is 1°C . The thermocline depth (i.e., 20°C isotherm) is highlighted.

with the Navy Coupled Ocean Data Assimilation (NCODA) to examine the relationship between SST and thermocline in the SCTR during IOD events. We also report the impacts that the SSTA asymmetries between PIOD and NIOD events have on the SSTA–D20A (D20 anomalies) relationship in the SCTR.

II. DATA AND METHODS

A. Observations

Daily $0.25^{\circ} \times 0.25^{\circ}$ gridded sea surface height anomaly (SSHA) data are acquired from Archiving, Validation, and Interpretation of Satellite Oceanographic data (AVISO) (<http://www.aviso.oceanobs.com>). AVISO computes the SSHA as deviations from the 1993–2012 mean sea level. This letter used monthly SSHA for January 1993 to December 2012, computed from the daily data.

Daily $0.05^{\circ} \times 0.05^{\circ}$ gridded Operational Sea surface Temperature and Sea Ice Analysis (OSTIA) system SST data are obtained from <http://www.myocean.eu.org> [12]. OSTIA data are produced from 4-km Advanced Very High Resolution Radiometer Pathfinder V5 data, 1-km Along Track Scanning Radiometer (ATSR) and Advanced ATSR multimission data, and *in situ* data from the International Comprehensive Ocean–Atmosphere Data Set archives. Monthly means are computed from the daily data.

B. HYCOM Reanalysis

Monthly outputs from a reanalysis version of the HYCOM for January 1993 to December 2012 are used in this letter. HYCOM is described in [13], and only a summary is presented here. The dynamic model used is HYCOM version 2.2 configured for the global ocean. The model has a nominal horizontal resolution of $1/12^{\circ}$ (~ 8 km at the equator) and 32 hybrid vertical layers.

The HYCOM data assimilation is done with the NCODA system [14]. NCODA uses a 3-D variational scheme implemented with the Incremental Analysis Update technique [15]. This technique is commonly used in reanalysis runs of the atmosphere or the ocean (see [16]). NCODA assimilates satellite altimeter and SST data. It also assimilates available *in situ* temperature and salinity data obtained from Argo floats, conductivity–temperature–depth profiles, expandable bathythermograph profiles, and moored buoys.

The surface forcing is the hourly 0.3125° National Center for Environmental Prediction (NCEP) Climate Forecast System Reanalysis (CFSR) wind, heat fluxes (computed using bulk formula), and precipitation fields [17]. The ocean reanalysis was initialized from a nonassimilative global HYCOM simulation spun-up to statistical equilibrium with climatology constructed from the NCEP CFSR forcing.

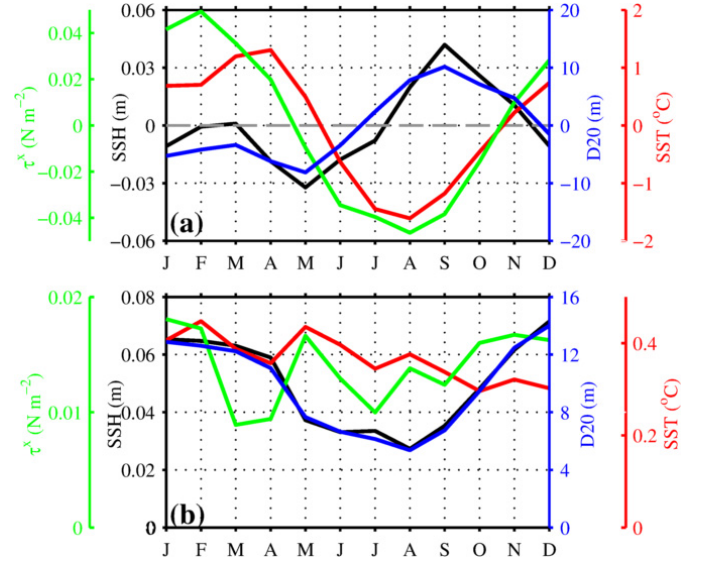


Fig. 2. (a) Seasonal variation of zonal wind stress (green line, $\text{N}\cdot\text{m}^{-2}$), sea surface height (black line, m), D20 (blue line, m), and SST' (red line, °C) averaged over the SCTR region. (b) Standard deviations of interannual anomalies averaged over the SCTR region.

C. Methods

Surface wind stress τ is obtained from CSFR wind speed \mathbf{U} using $\tau = \rho_a C_d |\mathbf{U}| \mathbf{U}$, where ρ_a is the density of air ($1.225 \text{ kg}\cdot\text{m}^{-3}$) and C_d is a constant drag coefficient (1.43×10^{-3}).

The 20°C isotherm depth (computed from HYCOM) is used as a proxy for the thermocline depth [18]. In the tropical oceans, SSH and D20 are strongly correlated. The D20 is a good approximation of the SSH in the SCTR ($r = 0.99$) with a shoaled thermocline corresponding to a low SSH and a deepened thermocline corresponding to a high SSH (Fig. 2). Thermocline feedback is a measure of the impact that D20 fluctuations have on the rate of SST changes and can be inferred from $-w'_e (\partial T' / \partial z)$, where w'_e and T' are vertical current (or Ekman pumping velocity) and temperature anomalies, respectively. $(\partial T' / \partial z)$ refers to the vertical gradient of the temperature anomalies

$$w_e = \nabla \times \left(\frac{\tau}{\rho_o f} \right) \quad (1)$$

where $\nabla \times \tau$ is the wind stress curl ($= \partial \tau^y / \partial x - \partial \tau^x / \partial y$), τ^x and τ^y are the zonal and meridional components of the wind stress, respectively. ρ_o is the seawater density ($1024 \text{ kg}\cdot\text{m}^{-3}$), f is the Coriolis parameter ($2\Omega \sin \phi$, where Ω is the angular velocity of the earth and ϕ is the latitude).

Finally, the heat content (HC) of the upper ocean is computed as

$$\text{HC} = \rho_o c_p \int_0^{D20} T(z) dz \quad (2)$$

where C_p is the specific heat capacity of seawater ($4 \times 10^3 \text{ J}\cdot\text{kg}^{-1}\cdot\text{K}^{-1}$) and $T(z)$ is the temperature at depth z .

As in [6], the dipole mode index (DMI), which is a measure of IOD activity, is computed as the difference between SSTA in the western Indian Ocean (50°E – 70°E , 10°S – 10°N) and that in the eastern Indian Ocean (90°E – 110°E , 10°S –equator). In this letter, the IOD years are those in which the DMI

exceeds 0.5 standard deviations for at least three months [18]. Composite means of PIOD events (1994, 1997, and 2006) and NIOD events (1996, 1998, 2005, and 2010) are formed to highlight the asymmetry and variability between positive and negative events and to understand the associated physical mechanisms during IOD events. Composite means of state variables during event years are represented as year (0) while those in the years immediately following the event years are classified as year (+1). Correlations presented in this letter are statistically significant above the 95% confidence level, unless otherwise noted.

III. RESULTS AND DISCUSSION

A. Overview of the SCTR

The seasonal cycle of the SCTR D20 is presented in Fig. 2(a). The thermocline ridge is prominent (i.e., shallow D20) during December–June, with the D20 attaining its minimum depth during the boreal spring (hereafter seasons refer to that of northern hemisphere) in May. At that time, it was ~ 8 m shallower than the annual mean depth. The shoaling of the D20 coincides with the strengthening of winds in the SCTR, suggesting that cyclonic wind stress curl-driven ocean dynamics are effecting changes to the thermocline depth. Conversely, the SCTR is weak (i.e., a deep D20) during summer and fall, with the D20 reaching a maximum depth during September, one month after the easterlies peak ($\sim 0.045 \text{ N} \cdot \text{m}^{-2}$) during August. D20 interannual anomalies are phase locked to the seasonal cycle with strongest variability occurring during the winter and weakest variability occurring during the summer [Fig. 2(b)]. Temperature in the surface layer undergoes strong seasonal variations with cooling during the summer and warming during the winter (Fig. 2).

B. Variability of the Subsurface Ocean

During PIOD events, anomalous easterly winds are observed in the southeastern tropical Indian Ocean in June, which peak during October–December in the SCTR region and persist till March of the following year (Fig. 3(a); [7]). These intensified winds cause anticyclonic wind stress curl and associated downwelling, which result in the deepening of the thermocline west of 90°E [Fig. 3(b) and (c)]. The D20 anomalies peak during December (0) and January (+1) and have their maximum near $\sim 65^\circ\text{E}$. The deepened thermocline depth anomalies then propagate westward through the SCTR region, reach the westernmost region during the peak of the PIOD event in October (0), and persist till the end of year (+1) even though the local winds weaken or reverse during most of year (+1). This propagation of D20 anomalies suggests remote influence by Rossby waves [19]–[21]. The positive D20 anomalies propagate westward with a phase speed of $0.14 \text{ m} \cdot \text{s}^{-1}$, which is slower than free mode-1 Rossby waves as they are forced by induced Ekman convergence that is a result of anticyclonic winds [1]. The persistence of anomalous D20 into the year after an event is noted early in the year of the PIOD events; e.g., the 1997 and 2006 PIOD events were preceded by the 1996 and 2005 NIOD events, respectively. It is seen that during January–March (0) of the PIOD composite means, the anomalous Ekman pumping is negative [Fig. 3(b)]. In spite of that, a shoaling thermocline is observed [Fig. 3(c)], possibly a result of a persistent shoaling thermocline from the prior year. The variability during NIOD events highlights the asymmetric relationship between the SCTR and different phases of the IOD.

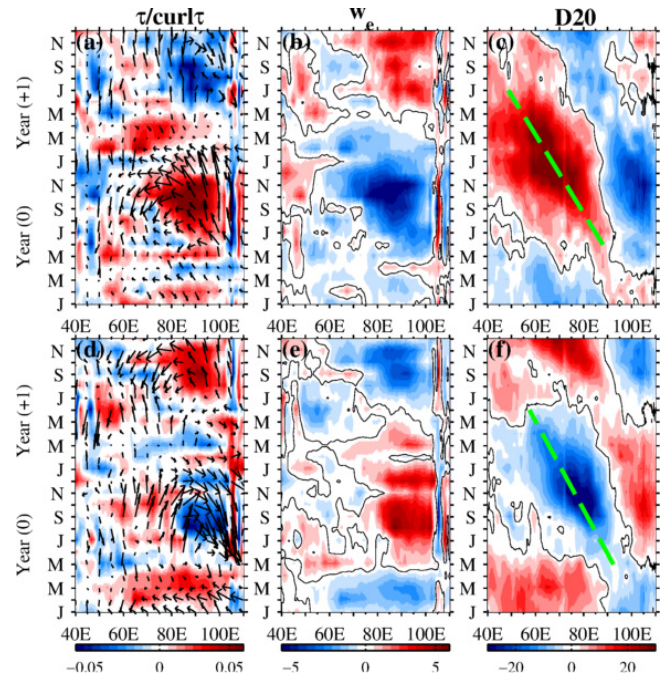


Fig. 3. Composite means of interannual anomalies of (a) wind stress curl (color shading, $\text{N} \cdot \text{m}^{-3}$) and wind stress (vectors, $\text{N} \cdot \text{m}^{-2}$), (b) Ekman pumping ($\times 10^{-6} \text{ m} \cdot \text{s}^{-1}$), and (c) D20 (m) during PIOD events. (d)–(f) Corresponding results during NIOD events. Green lines in (c) and (f) mark the Rossby first baroclinic wave propagation speeds. IOD event years (year 0) and the year following the IOD events (year +1) are shown. All variables are averaged over 5°S – 10°S .

In NIOD years, winds in the south equatorial Indian Ocean are favorable for downwelling, causing anomalous deepening of the D20 there, subsequently propagating westward and persists until the end of year (+1) [Fig. 3(d)–(f)]. Meanwhile, the usual predominantly easterly winds found further offshore in the southern tropical Indian Ocean reverse to westerlies and strengthen with the peak occurring just east of 80°E during October. This causes negative wind stress curl and a cyclonic flow that excites Ekman upwelling and causes upwelling Rossby waves in the central Indian Ocean just east of the SCTR [Fig. 3(d) and (e)]. This anomalously shallow D20 propagates westward at a phase speed of $0.12 \text{ m} \cdot \text{s}^{-1}$ (slower than during the PIOD events) and reaches the western boundaries by November (0). The shallow D20 anomalies persist until May–June of year (+1) unlike during the PIOD years when they persist until the end of year (+1).

The asymmetric influence of remote processes on the SCTR is captured in Fig. 4(a). The largest correlations between the wind stress curl and the D20 occur east of the SCTR. From Fig. 4(a), it is seen that the influence of anomalous wind stress curl on D20A just east of the SCTR during NIOD events is about three times stronger than the influence of anomalous wind stress curl on D20A during PIOD events, statistically significant at the 95% confidence level. As remotely generated Rossby waves are further influenced by Ekman pumping along their paths [22], there is a greater amplitude of reinforcing effect by anomalous winds on upwelling Rossby waves than on downwelling Rossby waves and hence a stronger remote influence during NIOD events than during PIOD events as less energy is needed to cause an uplift of a shallow D20 than that needed to cause an uplift of a deep D20 [10].

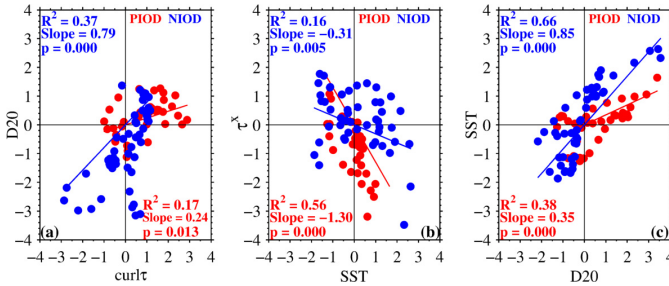


Fig. 4. Relationship between interannual anomalies of (a) wind stress curl and D20 east of the SCTR (averaged within 5°S – 10°S , 80°E – 90°E), (b) SST and zonal wind stress both averaged over the SCTR region (5°S – 10°S , 50°E – 80°E), and (c) D20 and SST both averaged over the SCTR region, during different phases of the IOD. Data are normalized by their respective standard deviations. Linear regression and correlations during PIOD events (red dots) and NIOD events (blue dots) are computed from the normalized data.

C. Variability of Thermocline and SST Relationship

We next examine the relation between temperature and D20 in the SWIO during different phases of the IOD. HC shows large variation as noted by some earlier studies (see [3], [19], [23]). DMI and SCTR HC anomalies are positively correlated with the strongest correlation ($r = 0.82$) occurring when DMI leads HC anomalies by three months (figure not shown). As noted earlier, IOD peaks in SON. During PIOD events, HC anomalies peak during January (+1) while they peak earlier in December (0) during NIOD events (Fig. 5). These months of peak anomalies overlap with the period when ENSO peaks in the Indian Ocean (i.e., NDJ), suggesting the influences of both the IOD and ENSO [8], [9].

The asymmetry in the HC anomalies between PIOD and NIOD events stands out during the peak and the months immediately following the IOD events. At the beginning of both PIOD and NIOD years, the amplitudes of the HC anomalies are quite comparable between the two events. At the peak of, and immediately following IOD events, however, the amplitude of the HC anomalies during PIOD is nearly twice as large as that of the NIOD events (Fig. 5). These anomalous HC patterns may be influenced by the asymmetry in the relation between the temperature and the zonal wind stress anomalies, which is statistically significant at the 95% confidence level [Fig. 4(b)]. An anomalous increase in temperature reinforces the magnitudes of anomalous easterlies during PIOD events ($\sim 4\times$) to a larger extent than an anomalous decrease in HC influence anomalous westerlies during NIOD events [Fig. 4(b)]. Thus, during PIOD events, a positive feedback can be inferred: the warmer SCTR SSTA feed back to the atmosphere, which strengthens the wind anomalies, intensifies atmospheric convection, and further induces anticyclonic circulation. This subsequently enhances the local Ekman pumping (which is directly proportional to the wind stress curl) and further deepens the thermocline and allows additional warming of the upper ocean. Furthermore, the enhanced temperature anomalies support additional precipitation, which increases the buoyancy of the upper ocean, and the creation of a barrier layer that further traps heat and warm the water column through ocean–atmosphere interactions [2], [10], [11].

Fig. 4(c) suggests that a nonlinear D20A–SSTA relation exists in the SCTR as a result of an asymmetry of the thermocline feedback mechanism during the phases of the IOD. This asymmetry between PIOD and NIOD events is statistically

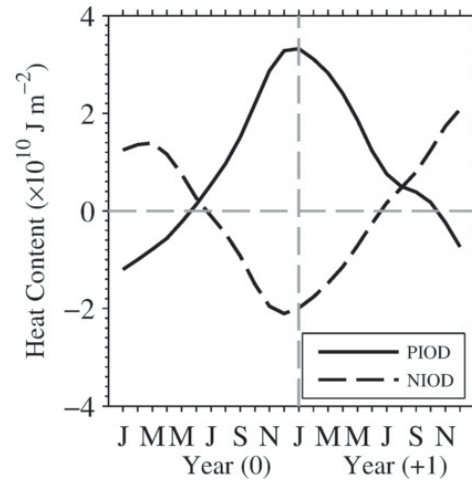


Fig. 5. Composite means of HC anomalies ($\times 10^{10} \text{ J} \cdot \text{m}^{-2}$) during PIOD (solid line) and NIOD (dashed line) events averaged over the SCTR.

significant at the 95% confidence level. The asymmetry causes a stronger SSTA response during NIOD events than that during PIOD as a shallower thermocline more effectively lowers the SST than a deeper thermocline permits raising the SST. The slopes from the respective linear regressions during IOD events [Fig. 4(c)] show a ratio of 0.85:0.35, suggesting that for the same absolute change in D20, there is a greater response to SST cooling when the thermocline is shoaling ($\sim 2.5\times$) than that to SST warming when the thermocline is deepening. These are in contrasts with the mechanisms that operate in the eastern Indian Ocean where stronger, asymmetric responses are observed during PIOD events [10], [11]. As the negative wind stress curl in the SCTR strengthens during NIOD events, the climatological shallow D20 becomes increasingly sensitive to the anomalous winds that act to further shoal it, bringing colder waters to the surface and reinforcing a decrease in SST. Conversely, during PIOD events, the thermocline depth deepens and suppresses the advection of colder subsurface waters, reducing its influence on the SST and causing a smaller thermocline feedback [Fig. 4(c)]. In summary, a shallow thermocline has a larger effect on surface changes than does a deeper thermocline as the latter implies a longer time lapse between the response of SSTAs to D20 changes, which in turn causes a weaker correlation between D20 and SSTAs [11].

IV. CONCLUSION

In this letter, the relationship between wind, D20, and SST have been studied for the SCTR region during PIOD and NIOD conditions. The existence of asymmetric environments between PIOD and NIOD events affect the subsurface–surface ocean interactions to different degrees, the consequence of which has not been extensively studied in the SWIO. We noted asymmetries in the relationships among wind stress curl, D20, and SST in the SWIO, synonymous with a Bjerknes-like feedback [10], [24]. During PIOD events, the SWIO experiences year round downwelling. The deep thermocline leads to increased HC anomalies and weakens the D20–SST coupling during PIOD events. An asymmetric relation between temperature and zonal wind stress anomalies during IOD events was found to reinforce easterly wind anomalies that occur during PIOD events to a much greater extent than westerly wind anomalies during NIOD events. As a result, during

PIOD events, a positive feedback exists, where the anticyclonic circulation is further strengthened, subsequently amplifies the local Ekman downwelling, and leads to a greater deepening of the thermocline and anomalous warming of the upper ocean.

The most intense D20 shoaling occurs just east of the SCTR and then propagates into the SCTR as Rossby waves. This remote influence on upwelling during NIOD events was found to be much greater than the remote influence on downwelling during PIOD events as anomalous westerlies are more effective at raising the D20 just east of the SCTR than anomalous easterlies are at lowering the D20 just east of the SCTR. The subsequent shallow thermocline in the SCTR induces subsurface cooling which reduces the magnitude of the HC and in turn causes a stronger D20–SST coupling during NIOD than that during PIOD events. The stronger coupling during NIOD than that during PIOD events is due to the asymmetry in the D20–SST feedback such that there is a greater impact by a shoaling thermocline to reduce SST than for a deepening thermocline to increase SST for the same change in thermocline depth, as implied by the linear regression of the SST and D20 relationship.

It has been shown that dynamics during unusual warm and cold events impact the year following these events [18], [25]–[27]. Chakravorty *et al.* [26] showed that when IOD and ENSO co-occur (as is the case of the events in this letter), the ENSO forcing continues to impact the effects of wind stress curl on Rossby waves beyond the peak seasons of the IOD events into year (+1). In this letter, we observed the D20 anomalies to persist beyond the IOD events, with longer persistence during PIOD than that during NIOD events. The stronger, asymmetric reinforcing effect of the anomalous zonal winds by the anomalous warm SST during PIOD events partly account for the longer persistence of the D20 anomalies into the year after the events than that during NIOD events [Fig. 4(b)].

ACKNOWLEDGMENT

The authors would like to thank Dr. E. Douglass and D. Franklin for helping with data acquisition. They would also like to thank the Editor and anonymous reviewers, whose comments contributed to the improvement of this letter. SSHA data were obtained from AVISO (<http://www.aviso.oceanobs.com>). OSTIA SST data were obtained from <http://www.myocean.eu.org>. The reanalysis outputs are from HYCOM experiments 19 and 19.1 run by the Naval Research Laboratory, Stennis Space Center, MS, USA. The output is publicly available at <http://hycom.org>.

REFERENCES

[1] S.-P. Xie, H. Annamalai, F. A. Schott, and J. P. McCreary, “Structure and mechanisms of south Indian Ocean climate variability,” *J. Climate*, vol. 15, pp. 864–878, Apr. 2002.

[2] O. Sayantani and C. Gnanaseelan, “Tropical Indian Ocean subsurface temperature variability and the forcing mechanisms,” *Climate Dyn.*, vol. 44, nos. 9–10, pp. 2447–2462, May 2015.

[3] J. C. Hermes and C. J. C. Reason, “Annual cycle of the South Indian Ocean (Seychelles-Chagos) thermocline ridge in a regional ocean model,” *J. Geophys. Res.*, vol. 107, no. C4, p. C04035, Apr. 2008, doi: [10.1029/2007JC004363](https://doi.org/10.1029/2007JC004363).

[4] T. Yokoi, T. Tozuka, and T. Yamagata, “Seasonal variation of the Seychelles Dome,” *J. Climate*, vol. 21, pp. 3740–3754, Aug. 2008.

[5] R. A. Madden and P. R. Julian, “Detection of a 40–50 day oscillation in the zonal wind in the tropical Pacific,” *J. Atmos. Sci.*, vol. 28, pp. 702–708, Jul. 1971.

[6] N. H. Saji, B. N. Goswami, P. N. Vinayachandran, and T. Yamagata, “A dipole mode in the tropical Indian Ocean,” *Nature*, vol. 401, pp. 360–363, Sep. 1999.

[7] P. J. Webster, A. M. Moore, J. P. Loschnigg, and R. R. Leben, “Coupled ocean-atmosphere dynamics in the Indian Ocean during 1997–98,” *Nature*, vol. 401, pp. 356–360, Sep. 1999.

[8] C. Gnanaseelan, A. Deshpande, and M. J. McPhaden, “Impact of Indian Ocean Dipole and El Niño/Southern oscillation wind-forcing on the Wyrтки jets,” *J. Geophys. Res.*, vol. 117, no. C8, p. C08005, Aug. 2012.

[9] G. Meyers, P. McIntosh, L. Pigot, and M. Pook, “The Years of El Niño, La Niña, and interactions with the tropical Indian Ocean,” *J. Climate*, vol. 20, no. 13, pp. 2872–2880, Jul. 2007.

[10] W. Cai and Y. Qiu, “An observation-based assessment of nonlinear feedback processes associated with the Indian Ocean Dipole,” *J. Climate*, vol. 26, pp. 2880–2890, May 2013.

[11] B. Ng, W. Cai, and K. Walsh, “The role of the SST-thermocline relationship in Indian Ocean Dipole skewness and its response to global warming,” *Sci. Rep.*, vol. 4, no. 6034, pp. 1–6, Aug. 2014, doi: [10.1038/srep06034](https://doi.org/10.1038/srep06034).

[12] J. Roberts-Jones, E. K. Fiedler, and M. J. Martin, “Daily, global, high-resolution SST and sea ice reanalysis for 1985–2007 using the OSTIA system,” *J. Climate*, vol. 25, pp. 6215–6232, Sep. 2012. [Online]. Available: <http://dx.doi.org/10.1175/JCLI-D-11-00648.1>

[13] E. J. Metzger *et al.*, “US Navy operational global ocean and Arctic ice prediction systems,” *Oceanography*, vol. 27, no. 3, pp. 32–43, Sep. 2014. [Online]. Available: <http://dx.doi.org/10.5670/oceanog.2014.66>

[14] J. A. Cummings and O. M. Smedstad, “Variational data assimilation for the global ocean,” in *Data Assimilation for Atmospheric, Oceanic and Hydrologic Applications*, vol. 2. Berlin, Germany: Springer-Verlag, 2013, ch. 13, pp. 303–343.

[15] S. C. Bloom, L. L. Takacs, A. M. da Silva, and D. Ledvina, “Data assimilation using incremental analysis updates,” *Monthly Weather Rev.*, vol. 124, pp. 1256–1271, Jun. 1996.

[16] Y. Ourmières, J.-M. Brankart, L. Berline, P. Brasseur, and J. Verron, “Incremental analysis update implementation into a sequential ocean data assimilation system,” *J. Atmos. Ocean Technol.*, vol. 23, pp. 1729–1744, Dec. 2006.

[17] S. Saha *et al.*, “The NCEP climate forecast system reanalysis,” *Bull. Amer. Meteorol. Soc.*, vol. 91, no. 8, pp. 1015–1057, Aug. 2010.

[18] E. S. Nyadjro and M. J. McPhaden, “Variability of zonal currents in the eastern equatorial Indian Ocean on seasonal to interannual time scales,” *J. Geophys. Res. Oceans*, vol. 119, no. 11, pp. 7969–7986, Nov. 2014, doi: [10.1002/2014JC010380](https://doi.org/10.1002/2014JC010380).

[19] T. Tozuka, T. Yokoi, and T. Yamagata, “A modeling study of interannual variations of the Seychelles Dome,” *J. Geophys. Res.*, vol. 115, no. C4, p. C04005, Apr. 2010, doi: [10.1029/2009JC005547](https://doi.org/10.1029/2009JC005547).

[20] L. L. Trenary and W. Han, “Intraseasonal-to-interannual variability of south Indian Ocean sea level and thermocline: Remote versus local forcing,” *J. Phys. Oceanogr.*, vol. 42, pp. 602–627, Apr. 2012.

[21] A. V. Rydbeck, T. G. Jensen, and E. S. Nyadjro, “Intraseasonal sea surface warming in the western Indian Ocean by oceanic equatorial Rossby waves,” *Geophys. Res. Lett.*, vol. 44, no. 9, pp. 4224–4232, May 2017, doi: [10.1002/2017GL073331](https://doi.org/10.1002/2017GL073331).

[22] Y. Masumoto and G. Meyers, “Forced Rossby waves in the southern tropical Indian Ocean,” *J. Geophys. Res.*, vol. 103, no. C12, pp. 27589–27602, Nov. 1998.

[23] T. G. Jensen, T. Shinoda, S. Chen, and M. Flatau, “Ocean response to CINDY/DYNAMO MJOs in air-sea-coupled COAMPS,” *J. Meteor. Soc. Jpn.*, vol. 93A, pp. 157–178, Dec. 2015. [Online]. Available: <http://doi.org/10.2151/jmsj.2015-049>

[24] J. Bjerknes, “A possible response of the atmospheric Hadley circulation to equatorial anomalies of ocean temperature,” *Tellus*, vol. 18, no. 4, pp. 820–829, Nov. 1966.

[25] C. Gnanaseelan, B. H. Vaid, and P. S. Politto, “Impact of biannual Rossby waves on the Indian Ocean Dipole,” *IEEE Geosci. Remote Sens. Lett.*, vol. 5, no. 3, pp. 427–429, Jul. 2008.

[26] S. Chakravorty, C. Gnanaseelan, J. S. Chowdary, and J.-J. Luo, “Relative role of El Niño and IOD forcing on the southern tropical Indian Ocean Rossby waves,” *J. Geophys. Res. Oceans*, vol. 119, no. 8, pp. 5105–5122, Aug. 2014, doi: [10.1002/2013JC009713](https://doi.org/10.1002/2013JC009713).

[27] C. Gnanaseelan and B. H. Vaid, “Interannual variability in the Biannual Rossby waves in the tropical Indian Ocean and its relation to Indian Ocean Dipole and El Niño forcing,” *Ocean Dyn.*, vol. 60, no. 1, pp. 27–40, Feb. 2010.